

MR perfusion and diffusion imaging in the follow-up of recurrent glioblastoma treated with dendritic cell immunotherapy: a pilot study

Matej Vrabc · Sofie Van Cauter · Uwe Himmelreich · Stefaan W. Van Gool · Stefan Sunaert · Steven De Vleeschouwer · Dušan Šuput · Philippe Demaerel

Received: 27 August 2010 / Accepted: 4 November 2010
© Springer-Verlag 2010

Abstract

Introduction This study aims to determine the potential value of MR-PWI and MR-DWI to differentiate immune therapy-induced inflammatory response from recurrent glioblastoma tumour growth. Both can present as contrast-enhancing lesions on conventional magnetic resonance imaging (MRI). **Methods** Patients with recurrent glioblastoma who could obtain a total or near-total resection were treated with dendritic cell immune therapy according to the HGG-IMMUNO-2003 trial. A retrospective analysis of 32 follow-up MRI examinations (mean follow-up time 21 months) in eight patients was performed for this pilot study. For the statistical analysis, the 32 examinations were divided into three groups: 0—obtained in patients that remained stable during the follow-up period, 1a—obtained in progressive-tumour patients at time points before definite progression and 1b—obtained in patients at or after progression.

Results Maximum lesional rCBV ratios were highest in group 1b (Student *t* test, 9.25 ± 2.68 ; $p < 0.001$) and were higher in group 1a (4.87 ± 1.61 , $p < 0.001$) compared to group 0 (1.22 ± 0.47). The minimum apparent diffusion coefficients (ADCs) in the contrast-enhancing regions were lower in group 1a ($0.62 \pm 0.06 \times 10^{-3} \text{ mm}^2/\text{s}$) than in group 0 ($1.03 \pm 0.43 \times 10^{-3} \text{ mm}^2/\text{s}$, $p = 0.01$) and higher in group 1b (0.76 ± 0.08) compared to 1a ($p = 0.02$). The minimum ADCs in the FLAIR-hyperintense region were lower in group 1a (0.62 ± 0.06 , $p = 0.02$) compared to group 0 (0.76 ± 0.16) but not significantly different in group 1b (0.68 ± 0.07) from groups 0 and 1a ($p = 0.33$, $p = 0.10$). The mean ADCs of the FLAIR-hyperintense region and the mean ADCs of the contrast-enhancing lesion were not significantly different.

Conclusion The maximum lesional rCBV ratios and minimum ADC values in the contrast-enhancing area are

Matej Vrabc and Sofie Van Cauter have equal contributions to this work.

M. Vrabc (✉)
Department of Radiology, University Clinical Center Ljubljana,
Zaloška 7,
1000, Ljubljana, Slovenia
e-mail: vrabc.m@gmail.com

S. Van Cauter · S. Sunaert · P. Demaerel
Department of Radiology, University Hospitals of Leuven,
Herestraat 49,
3000, Leuven, Belgium

U. Himmelreich
Biomedical NMR Unit/Molecular Small Animal Imaging Center,
Department of Medical Diagnostic Sciences,
Catholic University Leuven,
Herestraat 49,
3000, Leuven, Belgium

S. W. Van Gool
Department of Pediatric Neuro-oncology,
University Hospitals of Leuven,
Herestraat 49,
3000, Leuven, Belgium

S. De Vleeschouwer
Department of Neurosurgery,
University Hospitals of Leuven,
Herestraat 49,
3000, Leuven, Belgium

D. Šuput
Institute of Pathophysiology,
Faculty of Medicine, University of Ljubljana,
Zaloška 7,
1000, Ljubljana, Slovenia

potential radiological markers to differentiate between immune therapy-induced inflammatory response and recurrent glioblastoma tumour growth in glioblastoma patients treated with immune therapy.

Keywords MRI · Glioblastoma · Diffusion imaging · Perfusion imaging · Dendritic cell immunotherapy · Treatment monitoring

Introduction

Malignant gliomas (WHO grade III and IV gliomas) are the most common and aggressive type of brain tumours. Despite current multimodal treatment, consisting of surgery and concomitant radiochemotherapy, the prognosis of these patients remains poor. The life expectancy of patients with glioblastoma multiforme (GBM) treated with the current standard of care is on average 14 months [1]. As such, there is an obvious need for more effective, low-toxicity therapies.

Among innovative treatment strategies such as targeted therapy [2] and anti-angiogenesis therapy [3], immunotherapy has emerged as a promising and feasible treatment for inducing a long-term survival in at least a subpopulation of patients with high-grade gliomas. This is reflected in the increasing number of ongoing scientific research on immune therapy in high-grade brain tumours. A recent review has been published by Van Gool et al. [4]. Immunotherapy covers a broad field comprising several approaches, including passive immune therapy or stimulation, treatment with stimulated T cells and active specific immune therapy. For active specific immunotherapy, autologous dendritic cells (DC) are most commonly used as the vehicle for immunization [4].

DC are among the most potent immune stimulators, able to prime and activate adaptive immune T cells that can survey several tissues, including the central nervous system. In vivo primed T cells have the added potential to mount secondary memory responses. The primary goal of DC immune therapy is the induction of anti-tumour immunity while minimizing autoimmunity [5].

In the clinical setting, DC vaccines have essentially been used as an adjuvant therapy after surgical resection of the embedded tumour. Autologous DC are differentiated from harvested monocytes, cultured and loaded with antigens, i.e. whole tumour cell lysate from the patient's tumoural tissue obtained at surgical resection. They are matured in an ex vivo culture dish before intradermal administration [4].

Overall, these vaccines are well tolerated with few side effects. In many patients receiving vaccines, tumour progression was delayed and the median overall survival of these patients was prolonged and a substantial group of patients become long-term survivors [6–9]. The current

scope of research is mainly focused on optimization of vaccination schemes: boost vaccinations and methodology of vaccination administration in relapsed patients with glioblastoma who could obtain a total or near-total resection to optimize vaccination schemes.

In DC immunotherapy, the vaccine-induced inflammatory immune response commonly presents as a transient contrast enhancement in the brain parenchyma on magnetic resonance (MR) imaging. The contrast enhancement can be quite remarkable [10] and the differentiation between the inflammatory response, when presenting with contrast enhancement, and early tumour relapse can be challenging as the conventional MR imaging characteristics of both entities are similar.

In recent years, advances in MR technology have allowed us not only to visualize the macroscopic pathological anatomy of diseased organs but also to gain insight into the physiological characteristics such as vascularisation (perfusion-weighted MRI, PWI) [11] and cellular integrity (diffusion-weighted MRI, DWI) [12].

MR perfusion imaging parameters such as regional cerebral blood volume (rCBV) ratios have been shown to correlate with pathologically increased vascularity, which is characteristic for high-grade gliomas [13], and have been used to differentiate between enhancing lesions in radiation necrosis and recurrent tumour [14–16].

MR diffusion imaging has been applied for the diagnosis of high-grade glioma [17, 18]. Apparent diffusion coefficient (ADC) measurements have been shown to correlate with tumour cellularity [19], which correlates with tumour grade and has also been used for the differentiation of glioma recurrence and radiation injury [15, 20].

In this pilot study, we examine the role of perfusion-weighted and diffusion-weighted MR imaging in the follow-up of patients with recurrent GBM treated with immune therapy in order to assess the potential added value of the two techniques as radiological markers to differentiate between vaccine-induced inflammatory response and tumour recurrence.

Materials and methods

Patient selection

We retrospectively reviewed MR imaging studies from patients with GBM treated with immunotherapy according to the HGG-IMMUNO-2003 protocol in the University Hospitals of Leuven (HGG, high-grade glioma) [6].

Patients with recurrent GBM, who could obtain a total or near-total resection and be rapidly weaned from corticosteroids within 1 to 2 weeks after surgery, were included in the HGG-IMMUNO-2003 cohort comparison. The immune

therapy was administered as a single-treatment approach; hence, a change in the imaging appearance of the post-resection area such as the new onset of contrast enhancement was likely to represent either immune therapy-mediated effects or tumour progression [4, 9]. According to the HGG-IMMUNO-2003 protocol, conventional MR imaging time points were foreseen preoperatively, post-operatively before the start of the immune therapy, 1 month after therapy start and every following 3 months. The MR examinations were performed from May 2006 to May 2010. The patients gave informed consent to participate in the HGG-IMMUNO-2003 trial, which was approved by the institutional review board of the University Hospitals of Leuven.

The patient group consisted of eight individuals (six males, two females; age range 26–59; median age, 44 years). MR imaging was performed at the University Hospitals of Leuven, Belgium. All patients except one underwent the MR imaging session preoperatively in our hospital. All patients had conventional MR imaging follow-up according to the study protocol. MR examinations exclusively obtained within the scope of the HGG-IMMUNO-2003 trial were included in the study. Mean follow-up time was 20.5 months.

For the perfusion and diffusion imaging analysis, only MR examinations that were performed with both PWI and DWI were selected. A total of 32 follow-up studies, which represented DWI and PWI data from eight patients, obtained at two to eight different time points per patient, were analysed (Table 1).

Data acquisition and analysis

MR imaging in the subjects was performed on a 3T clinical MR system (Philips Achieva, Best, The Netherlands) with an eight-channel phased array head coil. The acquired images were transferred to an Apple Macintosh computer (Apple, Cupertino, USA), running Osirix open source image processing software [21].

Conventional MR sequences

The MR sequences were as follows: axial spin echo T2 (TR/TE=3,000/80 ms; slice/gap, 4/1 mm; TF, 10; FOV, 230×184 mm²), axial fluid attenuated inversion recovery (FLAIR) (TR/TE/TI=11,000/125/2,800 ms; slice/gap, 4/1 mm; FOV, 180×230 mm), axial spin echo T1 pre- and post-contrast administration (TR/TE=363/4.6 ms; slice/gap, 4.5/0 mm; FOV, 230 mm×184 mm²), sagittal spin echo T1 post-contrast administration (TR/TE: 367/4.6 ms; slice/gap, 4.5/0 mm; FOV, 230×218 mm²), coronal spin echo T1 post-contrast administration (TR/TE, 440/4.6 ms; slice/gap, 4.5/0 mm; FOV, 230×184 mm²).

PWI

Perfusion images were obtained with a gradient echo planar imaging sequence using the dynamic-susceptibility contrast-enhanced technique. The settings were as follows: TR/TE, 1,350/30 ms; slice/gap, 3/0 mm; number of slices, 24; dynamic scans, 60; EPI factor, 47; FOV, 200×200 mm; matrix, 112×109. Dynamic contrast agent-enhanced EPI were acquired during the first pass following a rapid injection of a 0.1-mmol/kg body weight bolus of meglumine-gadoterat (Dotarem, Guerbet) via a mechanical pump at a rate of 4 ml/s, followed by a 20-ml bolus of saline through a 20-gauge intravenous line to a cubital vein. Two-dimensional images were reconstructed using automatic calculation methods provided by the vendor. Concentration time curves of the first pass of the bolus were calculated and subsequently fitted with a gamma variate function [22] in order to derive the rCBV, regional cerebral blood flow (rCBF) and mean transit time. Corresponding maps were generated.

T1-weighted post-contrast images and FLAIR images were spatially co-registered to the rCBV maps. Regions of interest (ROIs) of the complete signal abnormality in the post-operative tumoural region—comprising both contrast-

Table 1 Overview of the patient data

	Age	Gender	Group	Total follow-up time with conventional MR (months)	Time from therapy start to progression (months)	Number of PWI and DWI follow-up time points
Patient 1	34	f	0	10		2
Patient 2	37	m	0	44		8
Patient 3	52	m	0	21		4
Patient 4	26	f	0	10		2
Patient 5	44	m	0	15		2
Patient 6	59	m	1	46	40	7 (1a, 6; 1b, 1)
Patient 7	45	m	1	10.5	7.5	3 (1a, 1; 1b, 2)
Patient 8	39	m	1	8	7	4 (1a, 2; 1b, 2)

m male, *f* female, *0* stable disease group, *1* progressive disease group, *1a* time points before distinct progression, *1b*—distinct progression

enhancing (if present) and FLAIR-hyperintense parts—were drawn and subsequently transferred onto the rCBV map under visual supervision to ensure correct spatial mapping. The procedure was repeated for all the slices on which FLAIR hyperintensity or contrast enhancement was perceived. Vessels were excluded from the ROIs by visual inspection of unprocessed perfusion images and spatially co-registered T2 and T1-weighted images.

The maximum rCBV value in the ROI was measured and the rCBV ratio was calculated by dividing the measured maximum lesional rCBV with the rCBV of the contralateral normal-appearing white matter.

DWI

Diffusion imaging was performed in the transverse plane using a single-shot spin-echo-echo planar imaging sequence with the following parameters: repetition time (ms)/echo time (ms), 3,529/70; diffusion gradient encoding in three orthogonal directions, $b=1,000$ s/mm²; slice thickness, 4 mm; slice gap, 0 mm; EPI factor, 57; diffusion gradient timing, 35.5/7 ms; Field of view, 230×230 mm² (with acquisition matrix, 128×128). After automatic pixel-by-pixel calculation, an ADC map was obtained.

For the diffusion analysis, the ADCs were measured separately in the contrast-enhancing part (when present) and in the surrounding FLAIR-hyperintense part. T1-weighted post-contrast images and FLAIR images were spatially co-registered to the ADC maps. ROIs of contrast-enhancing lesion were drawn on the T1-weighted post-contrast images and subsequently transferred onto the ADC map under visual supervision to ensure correct spatial mapping. The procedure was repeated for all the slices on which contrast enhancement was perceived. Similarly, ROIs were drawn on the spatially co-registered FLAIR images to include all hyperintense parts of the lesion. In both instances, great care has been taken to exclude any cystic or necrotic parts in the tumoural region. The minimum and mean ADCs of the contrast-enhancing and FLAIR-hyperintense part were calculated from the ROIs.

In the event of no demonstrable contrast enhancement present on the T1-weighted post-contrast images, the examination was excluded from the analysis of the contrast-enhancing lesions and included in the analysis of FLAIR-hyperintense regions only.

Statistical analysis

The 32 total examinations, performed in eight patients at two to eight different time points per patient (Table 1), were grouped into three groups. All examinations performed in patients that remained clinically and radiologically stable during the follow-up (mean follow-up period 20.5 months)

were grouped into group 0—stable. Examinations performed in patients that had tumour progression during the follow-up period (mean follow-up period 21.5 months) were divided into group 1a—examinations that had been performed at time points before distinct progression—and group 1b—examinations performed after progression.

To define distinct clinical or radiological progression, we adopted the criteria currently used in the clinical setting in the follow-up of recurrent GBM patients: a significant increase in contrast enhancement in or surrounding the resection area in more than two consecutive imaging time points on T1-weighted post-contrast images or a severe progressive clinical neurological deterioration [23].

The mean values of all the measured parameters—maximum lesional rCBV ratios, minimum and mean ADC values of the contrast-enhancing regions and minimum and mean ADC values of the FLAIR-hyperintense region—were calculated for all three groups. Box plots of the distribution of the measured values were drawn and group mean values were subsequently compared with Student *t* test. $P<0.05$ was considered to indicate a significant difference. IBM SPSS statistical software (IBM, Armonk, NY, USA) was used for the analysis.

Results

Three of the eight patients progressed during the study period. The time from the start of immune therapy to progression was from 7 to 40 months (median 7.5 months). Fourteen examinations of the total of 32 were obtained in progressive-tumour patients. Among them, nine examinations have been obtained at time points before distinct progression (group 1a) and five at or after progression (group 1b). All the examinations in progressive-tumour patients exhibited avid contrast enhancement.

The remaining five patients remained stable clinically as well as radiologically until the end of the study (10–44 months; median 15 months). All 18 examinations obtained in stable patients at various time points were included in group 0.

In three stable patients of five, no residual contrast enhancement was perceived after a certain time point: patient 1 did not have any demonstrable contrast enhancement at any point in the follow-up, and patients 2 and 3 did not have any perceivable contrast enhancement after 10.5 and 12.5 months from the start of immunotherapy, respectively. These examinations (ten from the total 32) with no contrast enhancement were not included in the analysis of ADC values of the contrast-enhancing regions and were included only in the analysis of FLAIR-hyperintense regions.

The calculated group means with standard deviations and ranges of the parameters measured are summarized in Table 2.

Table 2 Maximum lesional rCBV ratios, ADC values in contrast-enhancing regions and ADC values in FLAIR-hyperintense regions in the three groups

	Stable	Progressors	
	Group 0	Before progression, group 1a	After progression, group 1b
Maximum lesional rCBV ratio	1.22±0.47 (0.64–2.28)	4.87±1.61 (2.81–8.17)	9.25±2.68 (5.15–12.37)
Minimum ADC of contrast-enhancing part	1.03±0.43 (0.64–1.85)	0.62±0.06 (0.54–0.74)	0.76±0.08 (0.66–0.85)
Mean ADC of contrast-enhancing part	1.53±0.42 (1.02–2.11)	1.28±0.17 (1.03–1.43)	1.20±0.17 (1.02–1.41)
Minimum ADC of FLAIR hyperintensity	0.76±0.16 (0.54–1.17)	0.62±0.06 (0.54–0.74)	0.68±0.07 (0.62–0.80)
Mean ADC of FLAIR hyperintensity	1.31±0.28 (0.92–1.79)	1.40±0.16 (1.16–1.64)	1.30±0.15 (1.21–1.57)

ADCs are in 10^{-3} mm²/s

Group 0 stable disease, group 1a time points before distinct progression, group 1b distinct progression

Maximum rCBV ratios were significantly higher in group 1a (4.87±1.61), compared to stable patients (1.22±0.47, $p<0.001$). Maximum rCBV ratios were significantly higher in group 1b (9.25±2.68), compared to values measured in both stable patients ($p<0.001$) as well as group 1a ($p=0.017$). Figure 1 shows the distribution of rCBV values in the three groups.

The mean ADCs in the contrast-enhancing region were 1.53±0.42, 1.28±0.17 and 1.20±0.17×10⁻³ mm²/s in groups 0, 1a and 1b, respectively. There was a trend for the ADC values to be lower in group 1a than group 0 and lower in group 1b than 1a, but the difference was not significant ($p=0.11$, $p=0.43$). The difference between groups 0 and 1b was also insignificant ($p=0.08$).

Minimum ADCs in the contrast-enhancing regions were lower in group 1a (0.62±0.06×10⁻³ mm²/s) than in group 0 (1.03±0.43×10⁻³ mm²/s, $p=0.01$) and higher in group 1b

(0.76±0.08×10⁻³ mm²/s) compared to 1a ($p=0.02$). Figure 2 shows the distribution of measured minimum ADC values in the contrast-enhancing regions in the three groups.

The mean ADCs in FLAIR-hyperintense regions were similar across groups: 1.31±0.28, 1.40±0.16 and 1.30±0.15×10⁻³ mm²/s in groups 0, 1a and 1b, respectively.

Minimum ADCs in the FLAIR-hyperintense regions were lower in group 1a (0.62±0.06×10⁻³ mm²/s) compared to group 0 (0.76±0.16×10⁻³ mm²/s, $p=0.02$) but were not significantly different in group 1b (0.68±0.07×10⁻³ mm²/s) compared to either group 0 or 1a ($p=0.33$, $p=0.10$).

Discussion

In this pilot study, we evaluate the potential role of using dynamic susceptibility contrast-enhanced MR perfusion

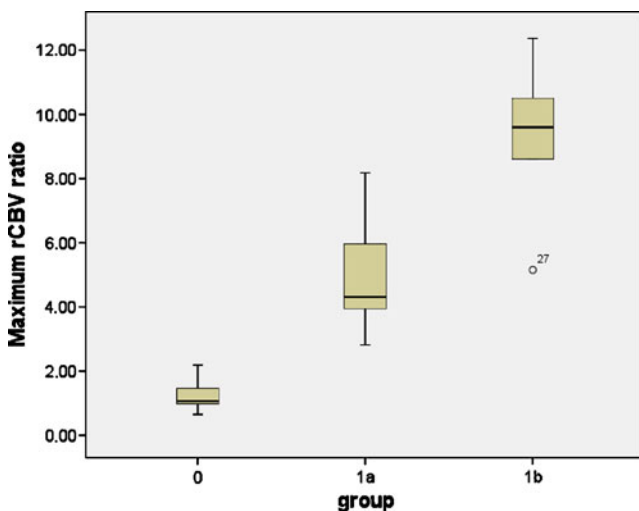


Fig. 1 Maximum rCBV ratios in the three groups (group 0: stable disease; group 1a: progressive-tumour patients at time points before distinct progression; group 1b: distinct progression). The *small circle* (27) represents an outlier (patient 7, second time point)

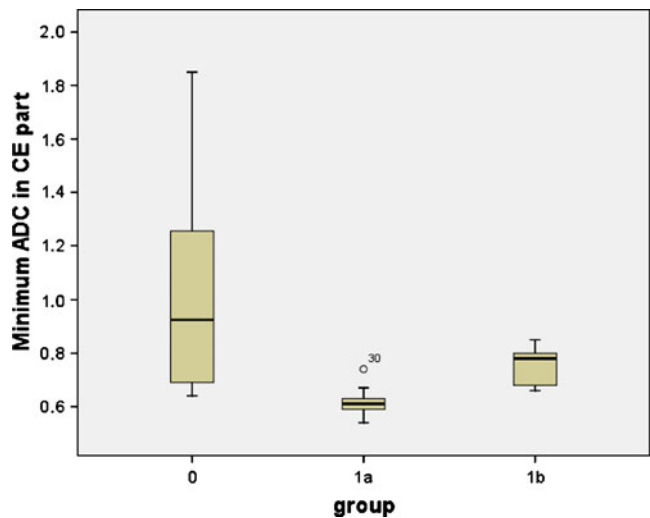


Fig. 2 Minimum ADCs in the contrast-enhancing regions in the three groups (group 0: stable disease; group 1a: progressive-tumour patients at time points before distinct progression; group 1b: distinct progression). The ADCs are in 10^{-3} mm²/s. The *small circle* (30) represents an outlier (patient 8, second time point)

and diffusion-weighted imaging in the follow-up of patients with recurrent GBM, treated with dendritic cell therapy as a single-treatment approach. To our knowledge, no data have been published regarding MR imaging-guided therapy monitoring of GBM patients treated with immune therapy.

Although high-grade gliomas (WHO grade III and IV gliomas) are categorized among the orphan diseases with a prevalence of four to seven per 100,000, they are the most common and aggressive brain tumours in adults. They manifest at every age with a peak incidence from 45 to 70 years and a predominance for males. Despite a multimodal-treatment approach consisting of surgery and combined radiochemotherapy, the prognosis of patients with high-grade glioma and, in particular, glioblastoma (WHO grade IV Gliomas) is extremely poor. Hence, the need for new therapies is clear. Immune therapy is emerging as a feasible treatment approach with low toxicity. Active specific immune therapy, in which dendritic cells are used as vehicle for immunization, is currently the scope of research in several groups. Although clinical evidence is emerging that survival can be prolonged in at least a subgroup of these patients, an adequate method for therapy monitoring is currently lacking. Adequate therapy monitoring is of utmost importance as this would allow for the timely detection of treatment failure, thereby permitting earlier changes in the treatment and therapeutic optimization.

Imaging follow-up in GBM patients is routinely performed with serial MRI scans. Several patients with malignant glioma, treated with the current standard of care of concomitant radiochemotherapy, have been described with subacute treatment-related reactions with or without clinical deterioration, showing diffuse enhancing lesions with variable perilesional oedema on MRI, suggestive of tumour progression [24–26]. Consecutive MR imaging elucidates that these alterations are not always related to tumour progression but represent a treatment-induced effect. This phenomenon has been referred to as “pseudo-progression”. Probably as a similar entity, comparable findings have been observed in ongoing trials on immune therapy for high-grade glioma [4]. MR imaging follow-up of GBM patients treated with immune therapy often demonstrates extensive and heterogeneous contrast enhancement along with variable perilesional edema and mass effects in the area of the tumour resection cavity after therapy administration. Hence, the differentiation between a vaccine-induced inflammatory immune reaction and early tumour recurrence remains challenging as the radiological characteristics of both entities are similar. As such, only further follow-up with repeat imaging and clinical correlation makes it possible to distinguish between these two conditions. PET scans with radiolabeled amino acid methionine may have an additional diagnostic value as this technique provides metabolic data for the observed alterations [27].

Many studies have shown promising results using PWI and DWI in glioma therapy monitoring [28–33]. Among the perfusion imaging parameters, we chose to measure rCBV, as it is the most robust and widely used quantitative variable derived from dynamic susceptibility-weighted contrast-enhanced MR imaging [32, 34]. There are a lot of published studies that have mainly analysed the perfusion and diffusion characteristics of the contrast-enhancing lesions [15, 30, 35–38]. As other studies have shown that tumour progression [39] or recurrence [40] may develop in the FLAIR-hyperintense parts of tumoural lesions, we decided to include the FLAIR-hyperintense regions into analysis. We assumed that we would run a risk of ignoring foci of possible tumour recurrence if rCBV and ADC values were solely analysed in the contrast-enhancing regions.

In our pilot study, we observed significantly higher maximum lesional rCBV ratios (9.25 ± 2.68) in progressive-tumour patients with a distinct tumour progression (group 1b) compared to patients who remained stable during the course of our observation (1.22 ± 0.47 , group 0). Furthermore, higher maximum lesional rCBV ratios (4.87 ± 1.61) than those found in stable patients were observed in individuals who were already progressive-tumour patients at the time points before the diagnosis of progression, based on clinical and conventional radiological characteristics, was made (group 1a). The measurements of maximum lesional rCBV ratios could potentially enable us to make the distinction between stable and progressive-tumour patients earlier than presently possible with established clinical and radiological criteria. Two patients with similar conventional imaging presentation at initial time points are presented in Figs. 3 and 4. One patient subsequently progressed; the other one remained stable until the end of the study.

Danchaivijitr et al. examined the longitudinal maximum rCBV ratios in the follow-up of conservatively treated glioma patients [39]. They found a progressive increase in maximum rCBV ratios in patients in which low-grade gliomas transformed to high-grade ones. The mean rCBV ratios at transformation were 5.36 ± 3.01 and elevated maximum rCBV ratios were measured in transforming patients as early as 18 months before transformation. This is similar to our findings regarding both the mean rCBV ratios and the observation of elevated rCBV ratios at imaging time points way before the diagnosis of distinct progression was made by the standard clinical and radiological criteria.

The range of maximum rCBV ratios we measured in the definite GBM progression group (5.15–12.37) corresponds to the values reported in the literature [13, 39, 41–43]. The mean maximum rCBV ratios that we obtained in the definite progression group (9.25 ± 2.68) were somewhat higher than the rCBV values of non-treated GBMs and

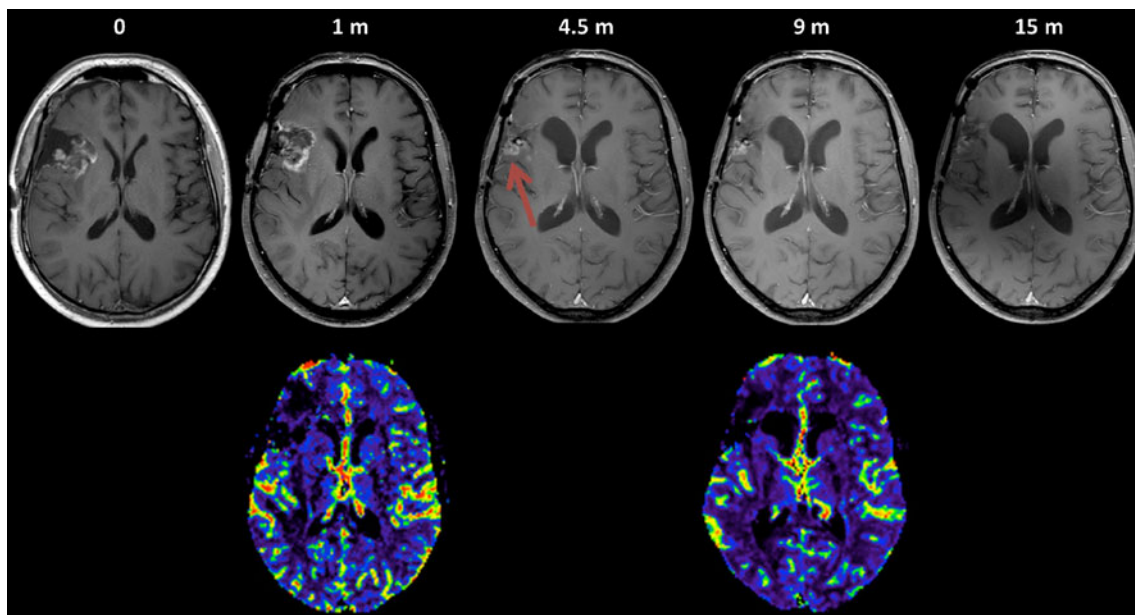


Fig. 3 Stable patient (patient 5). T1-weighted post-contrast images and rCBV maps at different time points in the follow-up. Time points in months. *0*—post-operatively, 20 days before the start of immune therapy. Some residual hematoma (T1-weighted pre-contrast images not shown) and contrast enhancement in the border of the resection cavity. *1 m*—1 month after the start of immune therapy. Some residual hematoma and more prominent contrast enhancement in the border of

the resection cavity. *4.5 m*—collapse of the resection cavity with a focus of parenchymal contrast enhancement in the lateral posterior border of the resection cavity (*arrow*); also present at 9 months. *15 m*—minimal residual contrast enhancement. The maximum rCBV ratios in the tumour resection cavity and bordering tissues remain low on both time points when perfusion imaging was performed

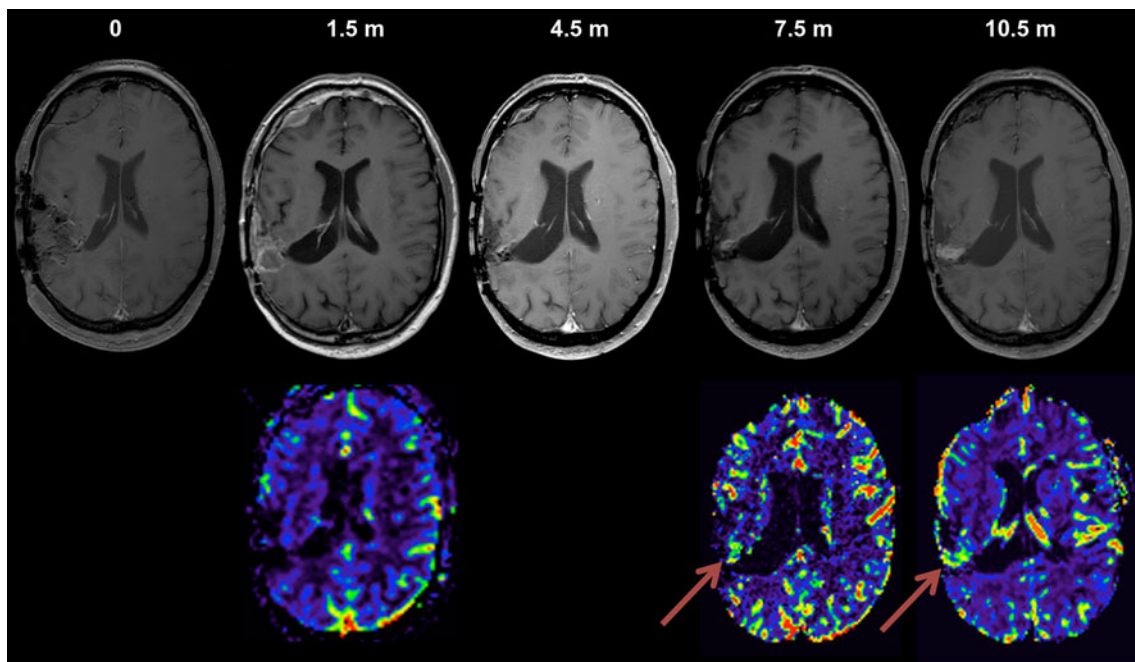


Fig. 4 Progressive-tumour patient (patient 7). T1-weighted post-contrast images and rCBV maps at different time points in the follow-up. Time points in months. *0*—post-operatively, 25 days before the start of immune therapy. *1.5 m*—1.5 months after the start of immune therapy; patchy contrast enhancement with some more linear enhancement of the resection cavity. *4.5 m*—minimal residual enhancement in the medial border of the resection cavity and a small increase in contrast enhancement in the latero-superior part (not

shown) of the resection cavity. *7.5 m*—discrete increase in contrast enhancement both in the antero-medial part (shown above) and latero-superior part (not shown). *10.5 m*—progressive increase in both the antero-medial part (shown above) and latero-superior part (not shown). At 7.5 and 10.5 months, respectively, a focus of elevated rCBV values can be appreciated on the rCBV maps (*arrows*), corresponding to a focus of nodular contrast enhancement on the T1-weighted contrast-enhanced images

high-grade gliomas reported by other groups: Sugahara et al. [13] reported a mean maximum rCBV ratio of 7.32 ± 4.39 for GBMs, Calli et al. reported 6.33 ± 2.03 for GBMs [41] and Yang et al. reported 6.10 ± 3.98 [43] for high-grade gliomas. The somewhat higher mean maximum rCBV ratios in our group of progressive GBM patients with a similar range of values could be due either to the small sample size, differences in the perfusion characteristics of recurrent tumour compared to non-treated tumours or higher MR field strength (3T).

Yamada et al. [44] reported an interesting pitfall of dynamic susceptibility contrast-enhanced MR perfusion-weighted imaging. Iron accumulations induce local field gradients through susceptibility. These field gradients induce T2*-shortening and may result in the underestimation of the measured CBV and CBF, in particular when gradient-echo sequences are applied in acquiring PWI. This phenomenon gives rise to errors in parameter calculation in case the degree of iron accumulation exerts some effect on the magnitude of signal change, and consequently the linear relationship between the magnitude of signal change and the tissue concentration of contrast material is not preserved. As haemorrhage and necrosis are well documented in high-grade gliomas [45], susceptibility artefacts induced by corresponding iron or heme depositions could possibly have affected our rCBV and rCBF calculations. Although this is a pertinent issue, we do not believe that our results are significantly influenced by this phenomenon. First of all, Yamada et al. report that susceptibility-induced errors in PWI parameter calculation only occur at a certain degree of iron accumulation, namely, when the degree of the T2*-shortening by iron accumulation interferes with the magnitude of signal change induced by the bolus of contrast agent. We checked for iron accumulation on the source images and had no evidence for important susceptibility artefacts. Furthermore, if this artefact would have been present in our data set, mainly the data from the stable patients would have been affected, as patients from this group are documented with lower values on rCBV and rCBF, compared to the results of the group of progressive-tumour patients.

We performed a literature search for MR perfusion characteristics of inflammatory diseases in the brain to find some reference values with which a comparison could be made with the measured maximum lesional rCBV ratios of inflammatory response in stable patients. We did not find any reports regarding MR perfusion values for immune therapy-induced inflammatory response. The inflammatory/infectious lesions of the brain that are pathologically distinct from therapy-induced inflammatory response, but have a higher prevalence and, as such, have been extensively studied, are brain abscesses. Abscesses have been shown to have lower rCBV ratios in the solid portion

of the lesion compared to the solid parts of centrally necrotic high-grade gliomas [46–51]. Erdogan et al. [48] found the mean rCBV in the abscess wall to be 0.76 ± 0.12 compared to 5.51 ± 2.08 in high-grade gliomas. The sizeable difference between the rCBV ratios reported in inflammatory lesions—abscesses and high-grade gliomas—is supportive to our findings of a large difference in maximum rCBV ratios between stable patients with therapy-induced inflammatory response and progressive-tumour patients.

In diffusion-weighted imaging, the minimum ADC values that we obtained in progressive-tumour patients (groups 1a and 1b) were similar to the minimum ADC values for non-treated GBMs reported in the literature by Kitis et al. ($0.70 \pm 0.16 \times 10^{-3} \text{ mm}^2/\text{s}$) [52].

ADC values have been shown to correlate with tumour cellularity [19] and grade [53, 54]. Higher cellularity, characteristic for high-grade gliomas, impedes molecular diffusional mobility and consequently causes lowering of the ADC.

For the ADC analysis, we opted to evaluate the contrast-enhancing region and FLAIR-hyperintense region separately, similarly to Jain et al. [29]. Our hypothesis is that, by choosing this method, we measured more objective values in the solid, contrast-enhancing part, less influenced by the amount of surrounding vasogenic oedema, while at the same time also not disregarding the possibly significant changes of ADC by the recurring tumour foci in the FLAIR-hyperintense part.

We observed lower minimum ADC values in both contrast-enhancing regions and FLAIR-hyperintense regions of patients in group 1a—progressive-tumour patients at time points before distinct progression—than in patients who remained stable. The lower ADC could be explained by increased cellularity in the developing recurrent tumour foci. In group 1b, the minimum ADCs in the contrast-enhancing regions were higher than the minimum ADCs measured in the contrast-enhancing regions in group 1a. This could be explained by the development of small necrotic regions as the tumour develops—too small to be completely excluded when manually drawing ROIs on the T1 post-contrast co-registered images.

We did not find any significant difference between mean ADC values across groups. In many patients, the contrast-enhancing lesion parts, as well as the FLAIR-hyperintense regions, were extensive. Tumour recurrence, on the contrary, most commonly starts to develop in small foci. The elevated ADC values in edematous white matter surrounding the small recurrent foci could explain why we did not find any significantly different measurements of mean ADC values across groups. By measuring the mean ADC value of the contrast-enhancing part or FLAIR-hyperintense ROI, the potentially lower ADC values of recurrent tumour foci

blended in the higher ADC values found in the more extensive white matter edema.

Similarly to MR perfusion characteristics, we did not find any reports in the literature on MR diffusion characteristics of immune therapy-induced inflammatory response in the brain for comparison. Other inflammatory diseases of the brain such as some types of encephalitis [55] and brain abscesses [48, 51, 56] exhibit lower ADC values than normal brain tissue. Contrary to maximum rCBV ratios, which are lower in abscesses than in high-grade tumours, the ADC values are lower both in high-grade tumours and inflammatory diseases than in normal brain tissue. The potentially lower ADC values in the vaccine-induced inflammatory response compared to normal brain tissue could represent a potentially confounding effect when trying to distinguish between the vaccine-induced inflammatory response and the recurrent tumour. Therefore, care should be taken when interpreting these results.

In this pilot study, MR imaging follow-up was retrospectively reviewed in patients with recurrent GBM, treated with active specific immune therapy as a single-treatment approach. We believe that maximum rCBV ratio measurements and minimum ADC values could be of potential use in the follow-up of GBM patients treated with immune therapy. In particular, the maximum rCBV ratios are a potentially good marker to indicate progressive or stable disease.

However, this study has several limitations. First, the sample size is small. Dendritic cell immune therapy is a novel treatment, with phase I and II studies being performed. In a recent review of dendritic cell studies for high-grade gliomas, the median sample size was 12 patients [57]. Some patients enrolled in the HGG-IMMUNO 2003 trial have their imaging follow-up performed at local hospitals on different MR scanners without perfusion imaging. Consequently, their imaging data could not be used for this study. We did not have a pathologic confirmation of tumour recurrence or immune therapy-induced inflammatory disease; we relied instead on serial clinical evolution and conventional radiological evaluation as our standard.

Conclusion

This pilot study, in which the role of advanced MR imaging techniques in therapy monitoring of GBM patients treated with immune therapy was examined, suggests that MR perfusion and diffusion-weighted imaging could be helpful to differentiate therapy-induced inflammatory response from recurrent tumour.

Larger prospective studies are planned to further evaluate the potential role of advanced MR imaging

techniques as biomarkers of treatment failure versus therapeutic success in immune therapy for high-grade gliomas.

Acknowledgments The immunotherapy programme is supported by the Olivia Hendrickx Research Fund (<http://www.olivia.be>), the Herman Memorial Research Fund (<http://www.hmrf.be>), the James E. Kearney Memorial Fund and gifts from private families and service clubs. Grants were obtained from “Stichting tegen Kanker,” IWT (TBM project), the Stem Cell Institute Leuven, the Emmanuel van der Schueren Fund, the International Union against Cancer, the Klinisch Onderzoeksfonds UZ Leuven and the Fund for Scientific Research—Flanders (FWO-V).

Conflict of Interest We declare that we have no conflict of interest.

References

1. Stupp R, Mason WP, van den Bent MJ et al (2005) Radiotherapy plus concomitant and adjuvant temozolomide for glioblastoma. *N Engl J Med* 352:987–996
2. Mason WP (2008) Emerging drugs for malignant glioma. *Expert Opin Emerg Drugs* 13:81–94
3. Gerstner ER, Duda DG, di Tomaso E, Sorensen G, Jain RK, Batchelor TT (2007) Antiangiogenic agents for the treatment of glioblastoma. *Expert Opin Investig Drugs* 16:1895–1908
4. Van Gool S, Maes W, Ardon H, Verschuere T, Van Cauter S, De Vleeschouwer S (2009) Dendritic cell therapy of high-grade gliomas. *Brain Pathol* 19:694–712
5. Banchereau J, Palucka AK (2005) Dendritic cells as therapeutic vaccines against cancer. *Nat Rev Immunol* 5:296–306
6. Rutkowski S, De Vleeschouwer S, Kaempgen E et al (2004) Surgery and adjuvant dendritic cell-based tumour vaccination for patients with relapsed malignant glioma, a feasibility study. *Br J Cancer* 91:1656–1662
7. Wheeler CJ, Black KL, Liu G et al (2008) Vaccination elicits correlated immune and clinical responses in glioblastoma multiforme patients. *Cancer Res* 68:5955–5964
8. Yu JS, Liu G, Ying H, Yong WH, Black KL, Wheeler CJ (2004) Vaccination with tumor lysate-pulsed dendritic cells elicits antigen-specific, cytotoxic T-cells in patients with malignant glioma. *Cancer Res* 64:4973–4979
9. De Vleeschouwer S, Fieuws S, Rutkowski S et al (2008) Postoperative adjuvant dendritic cell-based immunotherapy in patients with relapsed glioblastoma multiforme. *Clin Cancer Res* 14:3098–3104
10. De Vleeschouwer S, Van Calenbergh F, Demaerel P et al (2004) Transient local response and persistent tumor control in a child with recurrent malignant glioma: treatment with combination therapy including dendritic cell therapy. *Case report J Neurosurg* 100:492–497
11. Barrett T, Brechbiel M, Bernardo M, Choyke PL (2007) MRI of tumor angiogenesis. *J Magn Reson Imaging* 26:235–249
12. Le Bihan D, Turner R, Douek P, Patronas N (1992) Diffusion MR imaging: clinical applications. *AJR Am J Roentgenol* 159:591–599
13. Sugahara T, Korogi Y, Kochi M et al (1998) Correlation of MR imaging-determined cerebral blood volume maps with histologic and angiographic determination of vascularity of gliomas. *AJR Am J Roentgenol* 171:1479–1486
14. Barajas RFJ, Chang JS, Segal MR et al (2009) Differentiation of recurrent glioblastoma multiforme from radiation necrosis after external beam radiation therapy with dynamic susceptibility-

- weighted contrast-enhanced perfusion MR imaging. *Radiology* 253:486–496
15. Bobek-Billewicz B, Stasik-Pres G, Majchrzak H, Zarudzki L (2010) Differentiation between brain tumor recurrence and radiation injury using perfusion, diffusion-weighted imaging and MR spectroscopy. *Folia Neuropathol* 48:81–92
 16. Jain R, Narang J, Sundgren PM et al (2010) Treatment induced necrosis versus recurrent/progressing brain tumor: going beyond the boundaries of conventional morphologic imaging. *J Neurooncol* 100(1):17–29
 17. Baehring JM, Bi WL, Bannykh S, Piepmeyer JM, Fulbright RK (2007) Diffusion MRI in the early diagnosis of malignant glioma. *J Neurooncol* 82:221–225
 18. Kikuchi T, Kumabe T, Higano S, Watanabe M, Tominaga T (2009) Minimum apparent diffusion coefficient for the differential diagnosis of ganglioglioma. *Neurol Res* 31:1102–1107
 19. Chen J, Xia J, Zhou YC et al (2005) Correlation between magnetic resonance diffusion weighted imaging and cell density in astrocytoma. *Zhonghua Zhong Liu Za Zhi* 27:309–311
 20. Hein PA, Eskey CJ, Dunn JF, Hug EB (2004) Diffusion-weighted imaging in the follow-up of treated high-grade gliomas: tumor recurrence versus radiation injury. *AJNR Am J Neuroradiol* 25:201–209
 21. Rosset A, Spadola L, Ratib O (2004) OsiriX: an open-source software for navigating in multidimensional DICOM images. *J Digit Imaging* 17:205–216
 22. Belliveau JW, Kennedy DNJ, McKinstry RC et al (1991) Functional mapping of the human visual cortex by magnetic resonance imaging. *Science* 254:716–719
 23. Macdonald DR, Cascino TL, Schold SCJ, Cairncross JG (1990) Response criteria for phase II studies of supratentorial malignant glioma. *J Clin Oncol* 8:1277–1280
 24. Meyzer C, Dhermain F, Ducreux D et al (2010) A case report of pseudoprogression followed by complete remission after proton-beam irradiation for a low-grade glioma in a teenager: the value of dynamic contrast-enhanced MRI. *Radiat Oncol* 5:9
 25. Roldan GB, Scott JN, McIntyre JB et al (2009) Population-based study of pseudoprogression after chemoradiotherapy in GBM. *Can J Neurol Sci* 36:617–622
 26. Sanghera P, Perry J, Sahgal A et al (2010) Pseudoprogression following chemoradiotherapy for glioblastoma multiforme. *Can J Neurol Sci* 37:36–42
 27. Singhal T, Narayanan TK, Jain V, Mukherjee J, Mantil J (2008) ¹¹C-L-methionine positron emission tomography in the clinical management of cerebral gliomas. *Mol Imaging Biol* 10:1–18
 28. Hamstra DA, Chenevert TL, Moffat BA et al (2005) Evaluation of the functional diffusion map as an early biomarker of time-to-progression and overall survival in high-grade glioma. *Proc Natl Acad Sci U S A* 102:16759–16764
 29. Jain R, Scarpace LM, Ellika S et al (2010) Imaging response criteria for recurrent gliomas treated with bevacizumab: role of diffusion weighted imaging as an imaging biomarker. *J Neurooncol* 96:423–431
 30. Mangla R, Singh G, Ziegelitz D et al (2010) Changes in relative cerebral blood volume 1 month after radiation-temozolomide therapy can help predict overall survival in patients with glioblastoma. *Radiology* 256:575–584
 31. Padhani AR, Khan AA (2010) Diffusion-weighted (DW) and dynamic contrast-enhanced (DCE) magnetic resonance imaging (MRI) for monitoring anticancer therapy. *Target Oncol* 5:39–52
 32. Provenzale JM, Mukundan S, Barboriak DP (2006) Diffusion-weighted and perfusion MR imaging for brain tumor characterization and assessment of treatment response. *Radiology* 239:632–649
 33. Tomura N, Narita K, Izumi J et al (2006) Diffusion changes in a tumor and peritumoral tissue after stereotactic irradiation for brain tumors: possible prediction of treatment response. *J Comput Assist Tomogr* 30:496–500
 34. Cha S (2006) Update on brain tumor imaging: from anatomy to physiology. *AJNR Am J Neuroradiol* 27:475–487
 35. Aronen HJ, Perko J (2002) Dynamic susceptibility contrast MRI of gliomas. *Neuroimaging Clin N Am* 12:501–523
 36. Barajas RF, Chang JS, Sneed PK, Segal MR, McDermott MW, Cha S (2009) Distinguishing recurrent intra-axial metastatic tumor from radiation necrosis following gamma knife radiosurgery using dynamic susceptibility-weighted contrast-enhanced perfusion MR imaging. *AJNR Am J Neuroradiol* 30:367–372
 37. Bisdas S, Kirkpatrick M, Giglio P, Welsh C, Spampinato MV, Rumboldt Z (2009) Cerebral blood volume measurements by perfusion-weighted MR imaging in gliomas: ready for prime time in predicting short-term outcome and recurrent disease? *AJNR Am J Neuroradiol* 30:681–688
 38. Mitsuya K, Nakasu Y, Horiguchi S et al (2010) Perfusion weighted magnetic resonance imaging to distinguish the recurrence of metastatic brain tumors from radiation necrosis after stereotactic radiosurgery. *J Neurooncol* 99:81–88
 39. Danchavijitr N, Waldman AD, Tozer DJ et al (2008) Low-grade gliomas: do changes in rCBV measurements at longitudinal perfusion-weighted MR imaging predict malignant transformation? *Radiology* 247:170–178
 40. Stecco A, Pisani C, Quarta R et al (2010) DTI and PWI analysis of peri-enhancing tumoral brain tissue in patients treated for glioblastoma. *J Neurooncol*. doi:10.1007/s11060-010-0310-x
 41. Calli C, Kitis O, Yunten N, Yurtseven T, Islekel S, Akalin T (2006) Perfusion and diffusion MR imaging in enhancing malignant cerebral tumors. *Eur J Radiol* 58:394–403
 42. Sugahara T, Korogi Y, Kochi M, Ushio Y, Takahashi M (2001) Perfusion-sensitive MR imaging of gliomas: comparison between gradient-echo and spin-echo echo-planar imaging techniques. *AJNR Am J Neuroradiol* 22:1306–1315
 43. Yang D, Korogi Y, Sugahara T et al (2002) Cerebral gliomas: prospective comparison of multivoxel 2D chemical-shift imaging proton MR spectroscopy, echoplanar perfusion and diffusion-weighted MRI. *Neuroradiology* 44:656–666
 44. Yamada K, Gonzalez RG, O'Stergaard L et al (2002) Iron-induced susceptibility effect at the globus pallidus causes underestimation of flow and volume on dynamic susceptibility contrast-enhanced MR perfusion images. *AJNR Am J Neuroradiol* 23:1022–1029
 45. Kondziolka D, Bernstein M, Resch L et al (1987) Significance of hemorrhage into brain tumors: clinicopathological study. *J Neurosurg* 67:852–857
 46. Chawalparit O, Artkaew C, Anekthananon T, Tisavipat N, Charnchaowanish P, Sangruchi T (2009) Diagnostic accuracy of perfusion CT in differentiating brain abscess from necrotic tumor. *J Med Assoc Thai* 92:537–542
 47. Chiang IC, Hsieh TJ, Chiu ML, Liu GC, Kuo YT, Lin WC (2009) Distinction between pyogenic brain abscess and necrotic brain tumour using 3-tesla MR spectroscopy, diffusion and perfusion imaging. *Br J Radiol* 82:813–820
 48. Erdogan C, Hakyemez B, Yildirim N, Parlak M (2005) Brain abscess and cystic brain tumor: discrimination with dynamic susceptibility contrast perfusion-weighted MRI. *J Comput Assist Tomogr* 29:663–667
 49. Hakyemez B, Erdogan C, Bolca N, Yildirim N, Gokalp G, Parlak M (2006) Evaluation of different cerebral mass lesions by perfusion-weighted MR imaging. *J Magn Reson Imaging* 24:817–824
 50. Holmes TM, Petrella JR, Provenzale JM (2004) Distinction between cerebral abscesses and high-grade neoplasms by dynamic susceptibility contrast perfusion MRI. *AJR Am J Roentgenol* 183:1247–1252

51. Muccio CF, Esposito G, Bartolini A, Cerase A (2008) Cerebral abscesses and necrotic cerebral tumours: differential diagnosis by perfusion-weighted magnetic resonance imaging. *Radiol Med* 113:747–757
52. Kitis O, Altay H, Calli C, Yuntun N, Akalin T, Yurtseven T (2005) Minimum apparent diffusion coefficients in the evaluation of brain tumors. *Eur J Radiol* 55:393–400
53. Arvinda HR, Kesavadas C, Sarma PS et al (2009) Glioma grading: sensitivity, specificity, positive and negative predictive values of diffusion and perfusion imaging. *J Neurooncol* 94:87–96
54. Murakami R, Hirai T, Sugahara T et al (2009) Grading astrocytic tumors by using apparent diffusion coefficient parameters: superiority of a one- versus two-parameter pilot method. *Radiology* 251:838–845
55. Sawlani V (2009) Diffusion-weighted imaging and apparent diffusion coefficient evaluation of herpes simplex encephalitis and Japanese encephalitis. *J Neurol Sci* 287:221–226
56. Luthra G, Parihar A, Nath K et al (2007) Comparative evaluation of fungal, tubercular, and pyogenic brain abscesses with conventional and diffusion MR imaging and proton MR spectroscopy. *AJNR Am J Neuroradiol* 28:1332–1338
57. de Vleeschouwer S, Rapp M, Sorg RV et al (2006) Dendritic cell vaccination in patients with malignant gliomas: current status and future directions. *Neurosurgery* 59:988–999, discussion in 999–1000